Muscle weakness in *Ryr1*$^{I4895T/WT}$ knock-in mice as a result of reduced ryanodine receptor Ca^{2+} ion permeation and release from the sarcoplasmic reticulum

Ryan E. Loy,[1] Murat Orynbayev,[2] Le Xu,[3] Zoita Andronache,[2] Simona Apostol,[2] Elena Zvaritch,[4] David H. MacLennan,[4] Gerhard Meissner,[3] Werner Melzer,[2] and Robert T. Dirksen[1]

[1]Department of Pharmacology and Physiology, University of Rochester, Rochester, NY 14642
[2]Institute of Applied Physiology, Ulm University, D-89069 Ulm, Germany
[3]Department of Biochemistry and Biophysics, University of North Carolina, Chapel Hill, NC 27599
[4]Banting and Best Department of Medical Research, University of Toronto, Charles H. Best Institute, Toronto, Ontario, Canada M5G 1L6

The type 1 isoform of the ryanodine receptor (RYR1) is the Ca^{2+} release channel of the sarcoplasmic reticulum (SR) that is activated during skeletal muscle excitation–contraction (EC) coupling. Mutations in the *RYR1* gene cause several rare inherited skeletal muscle disorders, including malignant hyperthermia and central core disease (CCD). The human *RYR1*^{I4898T} mutation is one of the most common CCD mutations. To elucidate the mechanism by which RYR1 function is altered by this mutation, we characterized in vivo muscle strength, EC coupling, SR Ca^{2+} content, and RYR1 Ca^{2+} release channel function using adult heterozygous *Ryr1*$^{I4895T/+}$ knock-in mice (IT/+). Compared with age-matched wild-type (WT) mice, IT/+ mice exhibited significantly reduced upper body and grip strength. In spite of normal total SR Ca^{2+} content, both electrically evoked and 4-chloro-*m*-cresol–induced Ca^{2+} release were significantly reduced and slowed in single intact flexor digitorum brevis fibers isolated from 4–6-mo-old IT/+ mice. The sensitivity of the SR Ca^{2+} release mechanism to activation was not enhanced in fibers of IT/+ mice. Single-channel measurements of purified recombinant channels incorporated in planar lipid bilayers revealed that Ca^{2+} permeation was abolished for homotetrameric IT channels and significantly reduced for heterotetrameric WT:IT channels. Collectively, these findings indicate that in vivo muscle weakness observed in IT/+ knock-in mice arises from a reduction in the magnitude and rate of RYR1 Ca^{2+} release during EC coupling that results from the mutation producing a dominant-negative suppression of RYR1 channel Ca^{2+} ion permeation.

The Journal of General Physiology

INTRODUCTION

The RYR1 functions as the Ca^{2+} release channel in the skeletal muscle SR. The functional RYR1 SR Ca^{2+} release channel is a 2.3-megadalton homomeric assembly of four ~565-kD RYR1 subunits. Each RYR1 subunit is composed of a large N-terminal cytosolic "foot" region and six to eight transmembrane sequences located within the C-terminal portion of the protein (Du et al., 2002, 2004). By analogy with known K^+ channel structures, the selectivity filter of the RYR1 Ca^{2+} release channel is determined by a conserved hydrophobic sequence Gly-Ile-Gly (amino acids 4894-4895-4896 in mouse RYR1) (Zhao et al., 1999; Gao et al., 2000; Williams et al., 2001) located between the final two transmembrane domains. Fully assembled tetrameric Ca^{2+} release channels are arranged in regular arrays within the terminal cisternae of the SR (Franzini-Armstrong and Nunzi, 1983; Block et al., 1988; Franzini-Armstrong and Kish, 1995; Protasi et al., 1997). Activation of RYR1 Ca^{2+} release channels within these arrays during excitation–contraction (EC) coupling is controlled via a unique conformational interaction with the dihydropyridine receptor (DHPR; L-type Ca^{2+} channel), located in the adjacent transverse tubule membrane. DHPR–RYR1 conformational coupling is a bidirectional signaling interaction. Specifically, membrane depolarization triggers DHPRs to rapidly activate RYR1 channels to release SR Ca^{2+} (orthograde coupling), while the presence of RYR1 enhances L-type Ca^{2+} channel conduction and modifies the gating properties of the DHPR (retrograde coupling) (Nakai et al., 1996; Avila and Dirksen, 2000; Dirksen, 2002). Consistent with the notion that the DHPR and RYR1 Ca^{2+} channels are essential for skeletal muscle EC

R.E. Loy, M. Orynbayev, and L. Xu contributed equally to this paper.
Correspondence to Robert T. Dirksen: Robert_Dirksen@URMC.Rochester.edu

Abbreviations used in this paper: 4-CMC, 4-chloro-*m*-cresol; BTS, 4-methyl-*N*-(phenylmethyl)benzenesulfonamide; CCD, central core disease; DHPR, dihydropyridine receptor; EC, excitation–contraction; ECRE, elementary Ca^{2+} release event; FDB, flexor digitorum brevis; FDHM, full duration at half-maximum; FWHM, full width at half-maximum; IVCT, in vitro contracture test; MH, malignant hyperthermia; WT, wild type.

The Rockefeller University Press $30.00
J. Gen. Physiol. Vol. 137 No. 1 43–57
www.jgp.org/cgi/doi/10.1085/jgp.201010523

coupling, mutations in the DHPR and RYR1 proteins underlie several clinically distinct skeletal muscle disorders, including autosomal dominant malignant hyperthermia (MH), hypokalemic periodic paralysis, central core disease (CCD), and centronuclear myopathy (Jungbluth et al., 2007). Autosomal recessive mutations in RYR1 have also been linked to a form of multi-minicore disease (Jungbluth et al., 2005).

Functional testing of some of the large number of *RYR1* disease mutations identified to date has revealed three mechanistically distinct classes (Treves et al., 2008). One class of dominantly inherited *RYR1* mutations (termed "leaky" channel mutations) destabilizes the channel closed state and/or stabilizes the open state and, thus, sensitizes the channel to activation by a wide range of RYR1 triggers, including conformational activation by the DHPR and pharmacological activation by caffeine, 4-chloro-*m*-cresol (4-CMC), and volatile anesthetics (Tong et al., 1999; Avila and Dirksen, 2001). Physiological mechanisms in skeletal muscle exist to suppress inappropriate Ca^{2+} release. Loss of suppression can result from an MH mutation in either RYR1 (Robinson et al., 2006), $Ca_V1.1$ (Monnier et al., 1997), or type 1 calsequestrin deficiency (Dainese et al., 2009) that occurs in combination with an MH-triggering agent. Mechanisms proposed for enhanced RYR1 activity and escape from suppression of release include increased luminal Ca^{2+} sensitivity (Jiang et al., 2008), interdomain unzipping (Murayama et al., 2007), or altered regulation by cytosolic factors (Mickelson and Louis, 1996). We proposed that leaky channel mutations increase MH susceptibility and, if the defect is severe enough, can also lead to muscle weakness in CCD as a result of uncompensated RYR1 Ca^{2+} leak that results in SR Ca^{2+} depletion and a reduction in Ca^{2+} release during EC coupling (Tong et al., 1999; Dirksen and Avila, 2004). The second class of dominantly inherited *RYR1* mutations is proposed to reduce RYR1 Ca^{2+} release during EC coupling in a manner that occurs independently of a change in SR Ca^{2+} leak, Ca^{2+} store depletion, or RYR1 sensitization (Avila et al., 2001, 2003; Zvaritch et al., 2007). These mutations are expected to result in muscle weakness in the absence of MH susceptibility (Dirksen and Avila, 2002). The third class includes recessively inherited *RYR1* mutations that dramatically reduce RYR1 protein levels and severely lower Ca^{2+} release channel density within the junctional SR (Monnier et al., 2003; Zhou et al., 2006).

Lynch et al. (1999) identified a CCD mutation in the C-terminal region of RYR1 (I4898T) that is now considered to be one of the most common CCD mutations in humans. The highly conserved Ile4898 residue is located in the center of the selectivity filter of the RYR1 Ca^{2+} release channel (Gao et al., 2000). Based on functional reconstitution studies in myotubes derived from RYR1-null mice, we proposed that this mutation operates via the second class of mechanisms discussed above (reduced SR Ca^{2+} release without a change in leak, sensitivity, or store content) (Avila and Dirksen, 2001; Avila et al., 2001, 2003). However, other studies conducted after either heterologous expression in HEK293 cells (Lynch et al., 1999) or endogenous expression in B lymphocytes (Tilgen et al., 2001) and myotube cultures (Ducreux et al., 2004) derived from patients heterozygous for the I4898T mutation concluded that the I4898T mutation enhances RYR1 Ca^{2+} leak. Discrepancies between these reports most likely reflect differences between the preparations (purified RYRs, native cells, and homozygous/heterozygous expression), experimental approaches ($^{45}Ca^{2+}$ flux, Ca^{2+} measurements, and electrophysiology), and expression systems used (HEK293 cells, B lymphocytes, and human or dyspedic myotubes), none of which directly reflect RYR1 Ca^{2+} release channel function in fully differentiated adult skeletal muscle fibers.

To overcome these limitations, we compared in vivo muscle strength in adult wild-type (WT) and heterozygous *Ryr1*$^{I4895T/+}$ knock-in mice (IT/+) and correlated these findings with measurements of EC coupling, bidirectional DHPR–RYR1 conformational coupling, RYR1-mediated Ca^{2+} release, and SR Ca^{2+} content in single skeletal muscle fibers obtained from these animals. Single-channel studies of recombinant homotypic (WT:WT and IT:IT) and heterotypic (WT:IT) channels incorporated into planar lipid bilayers were completed to characterize the effect of the mutation on RYR1 channel Ca^{2+} conduction/selectivity. Our findings demonstrate that the I4895T mutation causes muscle weakness in IT/+ mice by reducing SR Ca^{2+} release as a result of a deficit in RYR1 Ca^{2+} ion permeation.

MATERIALS AND METHODS

Generation and handling of *Ryr1*$^{I4895T/+}$ knock-in mice

The generation and genotyping of inbred *Ryr1*$^{I4895T/wt}$ mice (IT/+) was described previously (Zvaritch et al., 2007). However, the animals used in this study were generated by inbreeding, not by backcrossing, as reported in Zvaritch et al. (2009). Animals were housed in a pathogen-free area at the University of Rochester or University of Ulm, and experiments were performed in accordance with procedures reviewed and approved by the local University Committees on Animal Resources. Mice were euthanized by regulated delivery of compressed CO_2 followed by cervical dislocation.

Assessment of in vivo muscle strength

In vivo muscle strength was evaluated using wire hanging (Ogura et al., 2001) and grip strength (Brooks and Dunnett, 2009; Matsuo et al., 2009) tests. The wire hanging test used an apparatus consisting of a taut horizontal wire attached to two stanchions 50 cm apart and 40 cm above a padded surface. Mice were held from the tail with forepaws free and then allowed to grasp the wire at a point equidistant from each stanchion. Once the wire was grasped, the mouse was released; each trial had a maximal duration of 60 s. Performance for each trial was scored between 0 and 5 as follows: 0, immediately fell off the bar; 1, hung onto bar

with two forepaws; 2, hung onto bar with two forepaws and attempted to climb onto the bar; 3, hung onto the bar with two forepaws and one or both hind paws; 4, hung onto the bar with all four paws and tail wrapped around the bar; 5, hung onto the bar with all four paws and tail wrapped around the bar and escaped onto one of the supports. Results for each mouse were averaged for 10 trials with 30 s of rest between each trial.

In vivo grip strength was evaluated for front paws only, back paws only, and all four paws together using an apparatus consisting of a stainless steel grid of 1-cm divisions connected to a digital force gauge (GTX; Dillon) set to record peak tensile force. The apparatus was arranged in a horizontal orientation, with the gripping grid placed on a horizontal track that minimizes frictional force. Each mouse was lowered to the apparatus, allowed to grasp the grid, and pulled slowly and continuously away from the force gauge until grip failed. Peak tensile force at the point of grip failure was recorded as grip strength. Each mouse performed five trials with 30 s of rest between each trial. Isolation of front or back paws was achieved by placing a smooth non-grip surface under the paws that were not being evaluated. Across all wire hanging and grip strength experiments, the average performance on the last trial was not significantly different from the average performance for the first trial, indicating the absence of significant fatigue during the tests. Wire hanging and grip strength experiments were performed using 4–5-mo-old male WT and IT/+ mice of similar weight, with measurements conducted and analyzed with the experimenter blinded to genotype.

Isolation of flexor digitorum brevis (FDB) muscle fibers

FDB muscle fibers were isolated from 4–6-mo-old mice as described previously (Beam and Knudson, 1988). In brief, FDB muscles were carefully removed from the hind paws and cleaned of associated connective tissue while bathed in a control Ringer's solution consisting of (in mM): 145 NaCl, 5 KCl, 2 $CaCl_2$, 1 $MgCl_2$, and 10 HEPES, pH 7.4. Muscles were then enzymatically dissociated in Ringer's solution supplemented with 1 mg/ml collagenase A (Roche) for 60 min while rocking gently at 37°C. Mechanical dissociation by trituration achieved final dispersal, enabling single fibers to be plated onto glass coverslips. Only fibers with a clean morphology, clear striations, and no signs of swelling or damage were used for recordings. All experiments were conducted within 8 h of fiber isolation.

Indo-1 Ca^{2+} measurements

Single FDB fibers were loaded with 6 µM indo-1 acetomethoxy ester (AM) in Ringer's solution for 30 min at room temperature. Fibers were then rinsed with indo-1 AM-free Ringer's solution supplemented with 25 µM 4-methyl-*N*-(phenylmethyl)benzenes ulfonamide (BTS; Tocris Bioscience), a skeletal muscle myosin II ATPase inhibitor, and incubated for >20 min to allow for de-esterification of the dye and inhibition of contraction. Cytosolic dye within a small rectangular region of the fiber was excited at 350 ± 10 nm using a 75-W xenon bulb and a high speed DeltaRAM illuminator (Photon Technology International). Fluorescence emission at 405 ± 30 nm (F_{405}) and 485 ± 25 nm (F_{485}) was collected (100 Hz) using a 40× (1.35 NA) oil-immersion fluorescence objective and a photomultiplier detection system (Photon Technology International) with results presented as the ratio of F_{405} and F_{485} ($R = F_{405}/F_{485}$). Electrically evoked Ca^{2+} transients were elicited using an electrical stimulus (8 V at 0.1 Hz) delivered using two extracellular electrodes filled with 1% agarose in 200 mM NaCl placed on either side of the cell of interest. Agonist-induced RYR1 Ca^{2+} release was triggered by rapid local application of 500 µM 4-CMC. A similar perfusion system was used for acquiring caffeine concentration–response curves. Fibers were sequentially exposed to 30-s applications of increasing concentrations of caffeine (0.1, 0.3, 0.6, 0.8, 1.0, 3.0, 10.0, 30.0, and 60.0 mM), with each concentration followed by a 45-s wash with control Ringer's solution. Data were plotted as the percentage of all fibers responding to a given concentration of caffeine and fit with a three-parameter Hill equation to determine Hill coefficient (n) and EC_{50} values. The maximum rate of 4-CMC–induced Ca^{2+} release was approximated by taking the peak of the first derivative of the indo-1 ratio (dR/dt).

Mag-fluo-4 Ca^{2+} measurements

The magnitude and kinetics of electrically evoked Ca^{2+} release were determined in FDB fibers using the low affinity (in vitro K_d = 22 µM; Invitrogen) Ca^{2+} dye mag-fluo-4 (Capote et al., 2005). For these experiments, single FDB fibers were loaded with 5 µM mag-fluo-4 AM in Ringer's solution for 30 min at room temperature, and then incubated for >20 min at room temperature in a dye-free Ringer's solution supplemented with 25 µM BTS. Mag-fluo-4 was excited at 480 ± 30 nm, and emission was monitored at 535 ± 40 nm using a 40× (1.35 NA) oil-immersion objective and collected at 10 kHz using a photomultiplier detection system. Fibers were stimulated with pulse trains at a frequency of 0.2 Hz using two flanking stimulation electrodes. Maximal ΔF/F values, where ΔF is the peak change in mag-fluo-4 emission from baseline and F is the baseline fluorescence recorded immediately before stimulation, for 10 different stimulation events were averaged and reported as a single value for each fiber. The 10 ΔF/F traces were differentiated, and peak values of the differential during the rising phase of the stimulated transients were averaged for each fiber (d[ΔF/F]/dt).

Fura-FF Ca^{2+} imaging

Responsiveness to 500 µM 4-CMC and total SR Ca^{2+} content were determined in single FDB fibers loaded with the low affinity (in vitro K_d = 6 µM; Invitrogen) ratiometric dye Fura-FF (Kimura et al., 2009). For these experiments, FDB fibers were loaded with 5 µM Fura-FF AM for 30 min at room temperature in control Ringer's solution. After loading, the bath solution was replaced with Ringer's solution supplemented with 50 µM BTS for 30 min at room temperature. Fura-FF–loaded fibers were alternately excited at 340 and 380 nm (510-nm emission) every 125 ms (20-ms exposure per wavelength and 4 × 4 binning) using a monochromator illumination system (Polychrome V; TILL Photonics). Images were captured using a high speed digital CCD camera (SENSICAM-QE; The COOKE Corporation) and TILL Vision software (TILL Photonics). Maximal RYR1-mediated Ca^{2+} release was determined after a 30–60-s application of 500 µM 4-CMC. After 4-CMC washout with Ringer's solution for 60 s, total store content was assessed using a 30-s application of a Ca^{2+} release cocktail (ICE) containing 10 µM ionomycin, 30 µM CPA, and 100 µM EGTA in a Ca^{2+}-free Ringer's solution. Maximal Fura-FF responsiveness was then determined after a final application of Ca^{2+} Ringer's solution to ensure that Fura-FF was not saturated during prior 4-CMC or ICE applications. The maximum rate of 4-CMC–induced Ca^{2+} release was approximated by taking the peak of the first derivative of the Fura-FF ratio (dR/dt).

Evaluation of elementary Ca^{2+} release events (ECREs)

Dissociation of single interosseous muscle fibers from adult WT and IT/+ mice was performed as described previously (Ursu et al., 2005). Fibers were loaded using 5 µM Fluo-4 AM (60 min at room temperature) and imaged using a 60× oil-immersion objective (1.4 NA; PlanApo) attached to an inverted microscope (Eclipse T300; Nikon) and a confocal scanner (Radiance 2000; Bio-Rad Laboratories). Fluorescence was excited at 488 nm and recorded after passing an HQ500LP emission filter. ECREs confined to the periphery of the fiber were induced by local application of a hyperosmotic Ringer's solution (440 mOsm with sucrose) and recorded in xy and line scan (xt) mode (Apostol et al., 2009).

Sequential xy images (512 × 512 pixels) were recorded at 1.5 Hz. To avoid photodynamic damage, the laser intensity was always set to the minimal power, providing reasonable fluorescence intensity, and when recording repeated xt images from the same region of the fiber, the y position was randomly changed within specified limits. In confocal line scan images (92 µm × 1,024 lines) acquired at 750 and 500 lines per second, the basal fluorescence level (F_0) was defined as the average intensity obtained from the lines with the lowest standard deviation. After F_0 subtraction, events rising above a preset threshold (0.6 times the standard deviation of the image) were automatically detected and analyzed to determine the following parameters: amplitude ($\Delta F/F_0$), full duration at half-maximum (FDHM), and full width at half-maximum (FWHM). The osmotic change often induced a transient rise in global fluorescence together with ECRE activity. Therefore, we performed line scanning for determining ECRE parameters 1 min after cessation of the hyperosmotic stimulus. Frames with clear elevation of basal fluorescence were excluded from the analysis. ECRE signal mass was calculated ($1.206*A*FWHM^3$) as described previously (Hollingworth et al., 2001). The formula assumes that the scan line runs through the location of the local Ca^{2+} release event and that the three-dimensional volume of the event is isotropic in space and approximated by the product of three Gaussian functions. Although no corrections were made for the contribution of out of focus events, the fractional contribution of such events should be similar in WT and IT/+ fibers.

Two-electrode voltage clamp

Two-electrode voltage clamp experiments (Ursu et al., 2004, 2005) were conducted to simultaneously record the magnitude, kinetics, and voltage dependence of L-type Ca^{2+} currents and Ca^{2+} release in interosseous muscle fibers dissociated from adult WT and IT/+ mice. In brief, isolated interosseous fibers were voltage clamped with a two-electrode system (Axoclamp 2B; Axon Instruments) and imaged using a fluorescence microscope (40×/0.75W objective; Axiovert 135 TV; Carl Zeiss, Inc.). The external bath solution contained (in mM): 130 TEA-OH, 130 HCH_3SO_3, 2 $MgCl_2$, 10 $CaCl_2$, 5 4-aminopyridine, 10 HEPES, 0.001 TTX, 5 glucose, and 0.05–0.1 BTS, pH 7.4.

In one series of experiments, fibers loaded with Fura-FF-AM (see above) were voltage clamped using two conventional microelectrodes filled with 3 M KCl. Ca^{2+} release was activated by 100-ms depolarizing pulses. In a second series of voltage clamp experiments, current was passed through a pipette of larger tip diameter (patch pipette) that was used for dialyzing the cell with a solution containing (in mM): 145 CsOH, 110 aspartic acid, 0.75 Na_2ATP, 4 MgATP, 1.5 $CaCl_2$, 10 HEPES, 15 EGTA, 0.2 fura-2, and 5 Na_2 creatine PO_4, pH 7.2. Fluorescence signals and L-type Ca^{2+} currents induced by 100-ms step depolarization were simultaneously recorded at 2 kHz. To construct Ca^{2+} current–voltage relationships, the L-type Ca^{2+} current magnitude was determined from the last 10 ms of each step depolarization. Ratiometric fura-2 Ca^{2+} transients were subjected to a removal model fit analysis (Melzer et al., 1986) with EGTA and fura-2 as the dominant Ca^{2+} buffers to calculate the flux of Ca^{2+} from the SR (Schuhmeier and Melzer, 2004; Ursu et al., 2005). The off-rate constant of fura-2 was fixed at 40 s^{-1} in this analysis. For determining flux amplitudes, we used a previous estimate of 40% loading of the cell with the pipette solution at the time of the measurements (Ursu et al., 2005). The voltage dependence of activation was described by Boltzmann functions, except for Ca^{2+} release, in which the Boltzmann term was multiplied by a linear term to account for a deviation at large depolarizations, as described previously (Ursu et al., 2005). Experimental temperature was 20–22°C, and the holding potential was −80 mV.

Expression and purification of WT and I4895T RYR1 channels

WT and mutant (I4897T mutation engineered into rabbit RYR1, which is analogous to I4898T in human RYR1 and I4895T in mouse RYR1) RYR1 cDNAs were transiently expressed in HEK293 cells, and proteoliposomes containing recombinant purified WT and mutant RYR1 channels were prepared as described previously (Xu et al., 2008).

Single-channel recordings

Single-channel measurements were performed using planar lipid bilayers containing a 5:3:2 mixture of bovine brain phosphatidylethanolamine, phosphatidylserine, and phosphatidylcholine (Xu et al., 2008). Proteoliposomes containing purified recombinant RYR1s were added to the cis (SR cytosolic side) chamber of a bilayer apparatus and fused in the presence of an osmotic gradient (250 mM cis KCl/20 mM trans KCl in 20 mM HEPES, pH 7.4, and 2 µM Ca^{2+}). After the appearance of channel activity, trans (SR lumenal) KCl concentration was increased to 250 mM. A strong dependence of single-channel activity on cis Ca^{2+} concentration indicated that the large cytosolic "foot" region faced the cis chamber of the bilayer. The trans side of the bilayer was defined as ground. Electrical signals were filtered at 2 kHz (0.5 kHz for Ca^{2+} currents at 0 mV), digitized at 10 kHz, and analyzed as described previously (Xu et al., 1999). To determine permeability ratios, single-channel activities were recorded in symmetrical 250 mM KCl solution with 10 mM Ca^{2+} on the trans side, and the reversal potential (E_{rev}) was measured. The permeability ratio of Ca^{2+} versus K^+ ions (P_{Ca}/P_K) was calculated using a modified form of the Goldman-Hodgkin-Katz equation:

$$E_{rev} = -\frac{RT}{F} Ln\left\{[K]^{\frac{1}{2}} \times \left([K] + 4\frac{P_{Ca}}{P_K}[Ca]\right)^{-\frac{1}{2}}\right\},$$

where [Ca] is the concentration of Ca^{2+} ions on the trans side, and [K] is the concentration of K^+ ions on the cis and trans sides.

Statistics

All average data are given as mean ± SEM. Statistical significance was evaluated using Student's *t* test, with statistical significance accepted at either *, $P < 0.01$ or †, $P < 0.05$.

Online supplemental material

Fig. S1 demonstrates that the caffeine sensitivity of SR Ca^{2+} release is modestly reduced in FDB fibers from IT/+ mice. Fig. S2 compares the frequency and properties of osmotic shock–induced ECREs in FDB fibers from control and IT/+ mice. The supplemental figures are available at http://www.jgp.org/cgi/content/full/jgp.201010523/DC1.

RESULTS

Prior studies in myotubes derived from newborn homozygous (IT/IT) mice indicate that homotetrameric I4895T Ca^{2+} release channels do not support either electrically evoked or ligand-induced SR Ca^{2+} release (Zvaritch et al., 2007). In contrast, because heterozygous mice (IT/+) survive, heterotetrameric WT:IT release channels presumably at least partially support EC coupling and SR Ca^{2+} release. Indeed, maximal in vitro twitch contraction and the rate of force development are reduced ∼30 and 15%, respectively, in soleus and lumbrical muscles from 2-mo-old heterozygous (IT/+) mice (Zvaritch et al., 2009). However, the underlying mechanism responsible for these reductions in strength has not been determined. Therefore, here we compared in vivo skeletal

muscle strength, EC coupling, Ca^{2+} signaling, and RYR1 channel function in adult WT and heterozygous *Ryr1*^{I4895T} (IT/+) knock-in mice.

Reduced in vivo muscle strength in IT/+ mice

We compared in vivo muscle strength in 4–5-mo-old male WT and IT/+ mice using both hanging task (Fig. 1 A) (Ogura et al., 2001) and grip strength (Fig. 1 B) (Brooks and Dunnett, 2009; Matsuo et al., 2009) tests. Grip strength and hanging tasks were used because performance in these tasks depends strongly on flexion of the digits, which involves the FDB and interosseous muscles used to assess EC coupling and RYR1 release channel function in subsequent single-fiber experiments (Figs. 2–5 and Figs. S1 and S2). A statistically significant ($P < 0.01$) reduction for both overall hanging task score (Fig. 1 A, left) and the percentage of trials in which mice were able to successfully escape to one of the stanchion supports (Fig. 1 A, right) was observed in 4–5-mo-old IT/+ mice. Consistent with these results, a statistically significant reduction in grip strength was observed in IT/+ mice. Specifically, a similar ∼25% reduction in grip strength quantified from either front paws only (Fig. 1 B, left), back paws only (Fig. 1 B, middle), or for all four paws (Fig. 1 B, right) was observed in IT/+ mice. Collectively, the results in Fig. 1 are consistent with a significant reduction of in vivo muscle strength in young adult IT/+ mice.

Reduced electrical- and ligand-induced Ca^{2+} release in fibers from IT/+ mice

Because a significant reduction in hanging task performance and grip strength was observed in IT/+ mice and the FDB muscle is one of the primary muscles used to flex the digits needed to hold onto a wire/grid, we hypothesized that in vivo muscle weakness in these behavioral tasks would be reflected as a reduction in Ca^{2+} release during EC coupling in single FDB muscle fibers. Therefore, we compared the magnitude and rate of electrically evoked and 4-CMC–induced Ca^{2+} release in single indo-1–loaded FDB muscle fibers from 4–6-mo-old WT and IT/+ mice (Fig. 2). For these experiments, voltage-gated Ca^{2+} release was activated by a brief train (0.1 Hz for 30 s) of supramaximal electrical stimuli delivered using extracellular stimulation electrodes flanking the fiber (Fig. 2 A, arrowheads). Shortly thereafter, fibers were rapidly exposed to a 30-s application of a maximal concentration of 4-CMC (500 µM), an RYR1 agonist (Fig. 2 A, black bars). Resting indo-1 fluorescence emission ratio (F_{405}/F_{485}) was significantly ($P < 0.05$) reduced in FDB fibers from IT/+ mice (WT: 0.53 ± 0.02, $n = 61$; IT/+: 0.47 ± 0.01, $n = 98$). Importantly, the average peak magnitudes of both electrically evoked (Fig. 2 B) and 4-CMC–induced (Fig. 2 C) Ca^{2+} transients were significantly ($P < 0.01$) reduced in FDB fibers from IT/+ mice.

Careful inspection of the time course of Ca^{2+} release during 4-CMC application revealed an apparent reduction in the rate of increase in the indo-1 ratio in FDB fibers from IT/+ mice (Fig. 2 D). We quantified this difference by comparing the peak value of the first derivative of the indo-1 ratio (dR/dt) during 4-CMC application in fibers from WT and IT/+ mice (Fig. 2 E). Compared with FDB fibers from age-matched WT mice, fibers from IT/+ mice exhibited a statistically significant ($P < 0.01$) 53.3 ± 14.2% reduction in peak dR/dt, consistent with a deficit in the maximum rate of SR Ca^{2+} release in FDB fibers of IT/+ mice.

Reduced rate of electrically evoked Ca^{2+} release in fibers from IT/+ mice

Results presented in Fig. 2 (D and E) demonstrate that the rate of RYR1-mediated Ca^{2+} release during 4-CMC activation is significantly reduced in FDB fibers from IT/+ mice. To determine whether a similar kinetic slowing of RYR1 Ca^{2+} release is also observed during EC

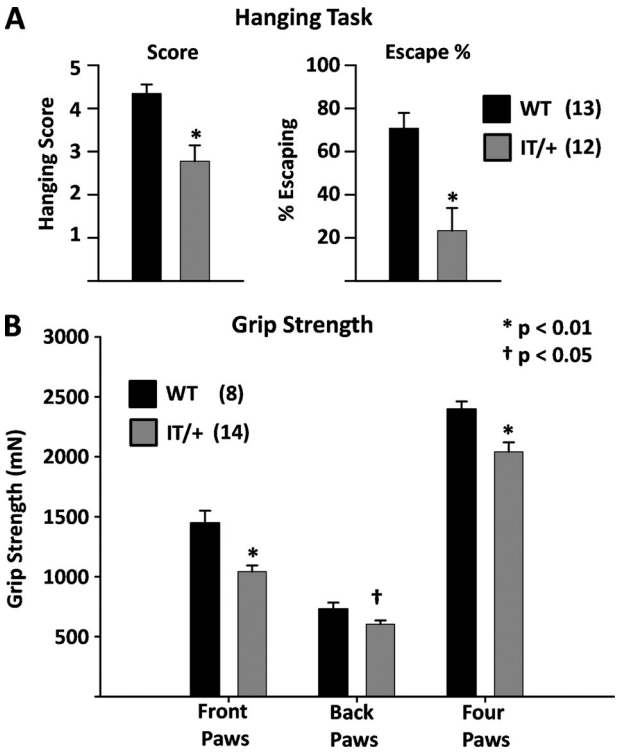

Figure 1. Reduced in vivo muscle strength in IT/+ mice. (A) In vivo hanging task determination of upper body strength in WT ($n = 13$ mice; black bar) and IT/+ ($n = 12$ mice; gray bar) mice. (Left) Average hanging scores from 10 trials/mouse (refer to Materials and methods for details). (Right) Percentage of hanging task trials in which WT and IT/+ mice successfully escaped to one of the stanchion supports. (B) Average grip strength (five trials/mouse) assayed from WT ($n = 8$ mice; black bar) and IT/+ ($n = 14$ mice; gray bar) mice using a digital force gauge (GTX; Dillon) set to record the peak tensile force generated by mice gripping a metal grid while being pulled away until grip fails. *, $P < 0.01$; †, $P < 0.05$.

coupling, we compared the magnitude and kinetics of electrically evoked Ca^{2+} release in FDB fibers from WT and IT/+ mice using mag-fluo-4, a rapid, low affinity Ca^{2+} dye with binding kinetics sufficient to accurately track Ca^{2+} transient time course during EC coupling (Capote et al., 2005). For the experiments shown in Fig. 3 A, mag-fluo-4–loaded FDB fibers from WT and IT/+ mice were stimulated with a brief train of supramaximal electrical stimuli, as described above. To maximize resolution of the electrically evoked transients, changes in mag-fluo-4 emission were recorded at high bandwidth (10 kHz), and movement artifacts were eliminated by inhibiting contraction with 25 µM BTS. Box plots of peak electrically evoked mag-fluo-4 fluorescence (ΔF/F) for all WT ($n = 53$) and IT/+ ($n = 56$) fibers are shown in Fig. 3 C. The box plots confirm that the magnitude of electrically evoked Ca^{2+} release is significantly reduced in FDB fibers from IT/+ mice. The maximum rate of electrically evoked Ca^{2+} release was approximated from the peak of the first derivative of the mag-fluo-4 fluorescence (d[ΔF/F]/dt) (Fig. 3 B). Box plots of the peak differential determined during electrically evoked Ca^{2+} release for all WT ($n = 53$) and IT/+ ($n = 56$) fibers are shown in Fig. 3 D. The results indicate that the maximum rate of RYR1-mediated Ca^{2+} release during EC coupling is significantly reduced in fibers from IT/+ mice. The reduction in the peak magnitude (Fig. 3 C) and rate (Fig. 3 D) of electrically evoked Ca^{2+} transients in fibers from IT/+ mice was also confirmed after averaging responses on a per mouse basis (Fig. 3, E and F).

Unaltered Ca^{2+} store content in fibers from IT/+ mice

The observed reduction in magnitude and rate of RYR1-mediated Ca^{2+} release in FDB fibers from IT/+ mice could potentially reflect a reduction in releasable SR Ca^{2+} content. Indeed, an increase in both ER/SR Ca^{2+} leak and store depletion has been reported in both B lymphocytes (Tilgen et al., 2001) and myotube cultures (Ducreux et al., 2004) derived from patients heterozygous for the I4898T mutation in human RYR1. Therefore, we compared intracellular Ca^{2+} store content in FDB fibers from WT and IT/+ mice using a rapid Ca^{2+} release cocktail (ICE) consisting of 10 µM ionomycin, 30 µM CPA, and 100 µM EGTA/0 Ca^{2+} (Zvaritch et al., 2007). To obviate potential problems related to rapid ICE-mediated myoplasmic Ca^{2+} increase, intracellular Ca^{2+} was measured using a low affinity ratiometric dye (Fura-FF), and movement/contraction was inhibited

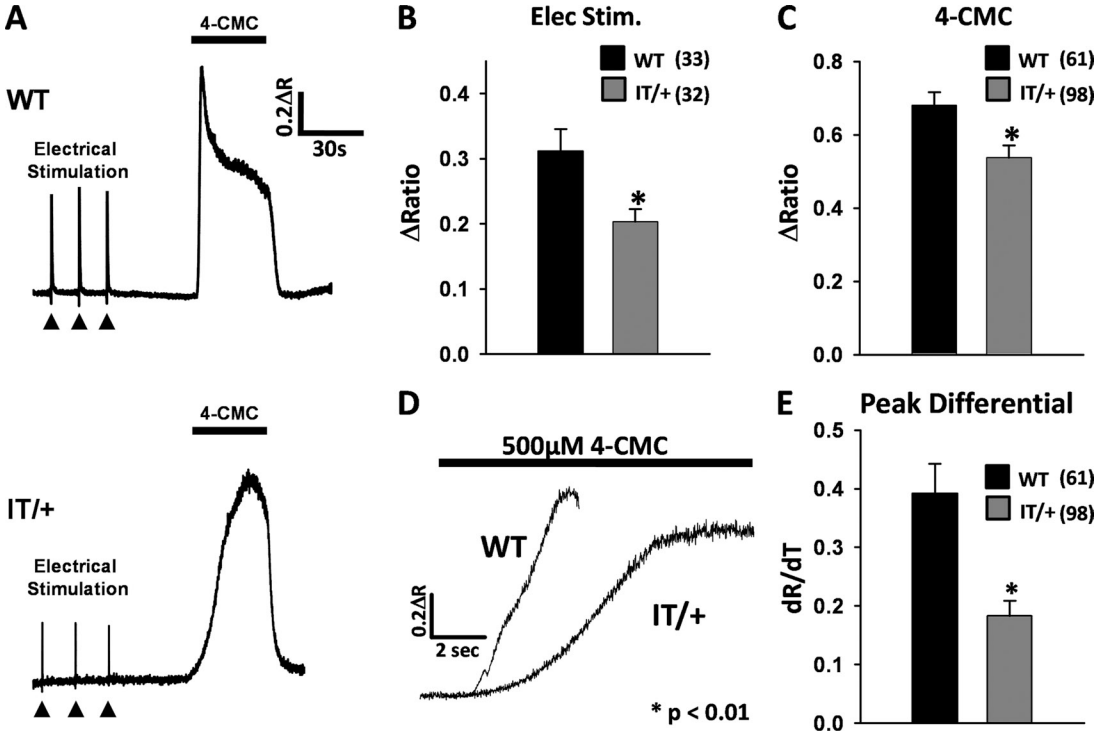

Figure 2. Reduction of electrically evoked and 4-CMC–induced RYR1-mediated Ca^{2+} release in indo-1–loaded FDB fibers from IT/+ mice. (A) Representative indo-1 ratio traces for FDB fibers from WT (top) and IT/+ (bottom) mice during successive electrical stimulation (arrowheads) and the application of 500 µM 4-CMC (black bar). (B) Average (±SEM) peak electrically evoked Ca^{2+} transients in FDB fibers from WT ($n = 33$; black bar) and IT/+ ($n = 32$; gray bar) mice. (C) Average (±SEM) peak 4-CMC–induced Ca^{2+} responses in FDB fibers from WT ($n = 61$; black bar) and IT/+ ($n = 98$; gray bar) mice. (D) Expanded time course of the rising phase of the indo-1 ratio during the application of 500 µM 4-CMC in representative FDB fibers from WT and IT/+ mice. For clarity, each trace is truncated after reaching the peak response. (E) Average (±SEM) peak of the first derivative of the rising phase of 4-CMC–induced Ca^{2+} responses in FDB fibers from WT ($n = 61$; black bar) and IT/+ ($n = 98$; gray bar) mice. *, $P < 0.01$.

by including 50 µM BTS in all solutions. Fura-FF–loaded fibers were then challenged sequentially with 500 µM 4-CMC, a 60-s wash with control Ringer's solution, and then the application of ICE to liberate Ca^{2+} rapidly from intracellular stores (Fig. 4 A). The results confirm that the magnitude and rate of 4-CMC–induced Ca^{2+} release are significantly ($P < 0.05$) reduced in FDB fibers from IT/+ mice (Fig. 4, B and C) and, importantly, that this reduction was not a result of a decrease in SR Ca^{2+} store content (Fig. 4 D).

Unaltered release channel sensitivity to activation in fibers of IT/+ mice

We investigated DHPR–RYR1 coupling under voltage clamp conditions in isolated interosseous fibers from WT and IT/+ mice. Using a two-electrode voltage clamp device, the membrane potential was held at −80 mV and Ca^{2+} release was activated by depolarizing pulses. In one series of experiments, we used high resistance electrodes and a membrane-permeant, low affinity Ca^{2+} indicator (Fura-FF-AM) to minimally disturb the intracellular environment. Ratiometric Ca^{2+} signals activated by large depolarizations (to +50 mV) of 100-ms duration showed a significant 22% reduction in peak amplitude in IT/+ fibers (mean ΔR decreased from 0.611 ± 0.040 [$n = 29$] to 0.474 ± 0.044 [$n = 37$; $P < 0.05$]), consistent with the reduction in electrically evoked Ca^{2+} release in intact cells described in Figs. 2 and 3. A second series of experiments was performed to specifically study the voltage dependence of both DHPR-mediated Ca^{2+} entry and SR Ca^{2+} release, and to compare their properties in the same fibers. To this end, the current passing micropipette had a larger tip diameter to allow intracellular dialysis with the artificial solution in the pipette. The dialysis facilitates the recording of the L-type Ca^{2+} current and the determination of the time course of Ca^{2+} release. The pipette solution contained the Ca^{2+} indicator (fura-2) and 15 mM EGTA, which together served as the dominant Ca^{2+} buffers. Although Ca^{2+} current and Ca^{2+} conductance showed very similar amplitude and voltage dependence (Fig. 5, A and B), the mean amplitude of the peak Ca^{2+} signal was significantly reduced (36% at +50 mV) in the IT/+ fibers (Fig. 5 C). To characterize Ca^{2+} release in more detail, we performed a Ca^{2+} removal analysis (Melzer et al., 1986) in the decay phases of repetitive pulses. The result was used to estimate the depolarization-activated Ca^{2+} release flux from the SR (Ursu et al., 2005). The mean maximal value of the flux was 23% smaller in IT/+ fibers compared with WT fibers (see Fig. 5 legend), but this difference was not statistically significant. A likely reason is the variability in the efficiency of intracellular dialysis and deviations from the assumed fixed EGTA concentration in the fiber (refer to Materials and methods), because the amplitude estimate in the release calculation is linearly dependent on the dominating

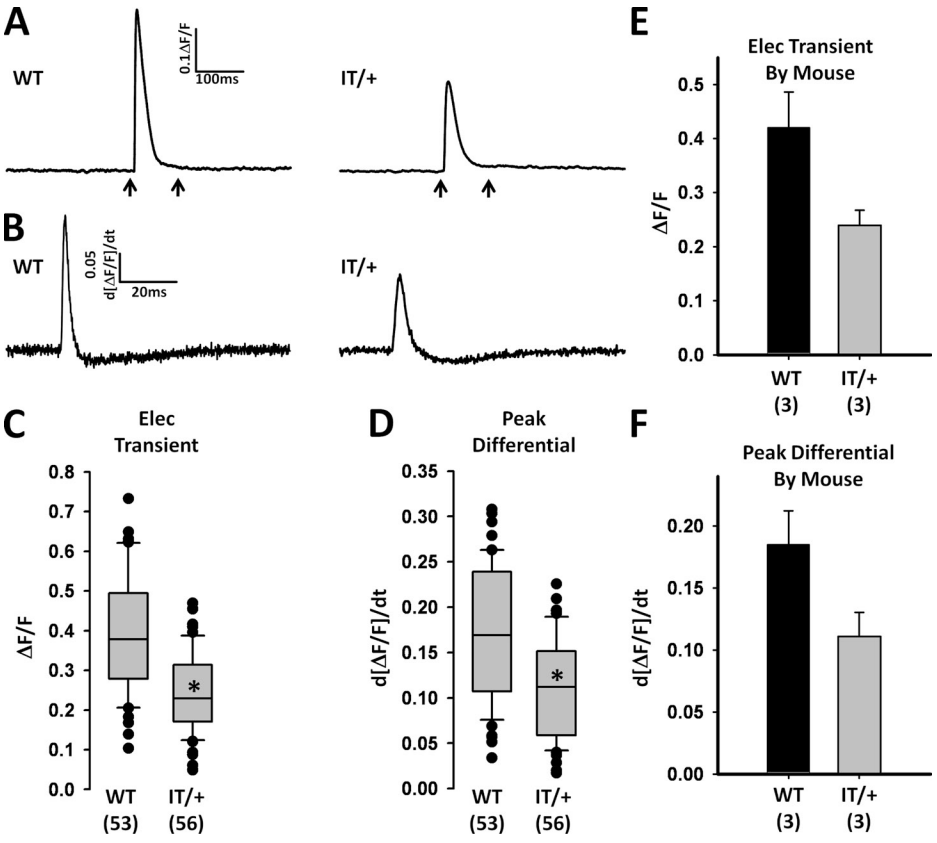

Figure 3. Slowed rate of electrically evoked Ca^{2+} transients in mag-fluo-4–loaded FDB fibers from IT/+ mice. (A) Representative single electrically evoked Ca^{2+} transients elicited during a brief 0.1-Hz train of stimulation in FDB fibers from WT (left) and IT/+ (right) mice. Sampling rate was 10 kHz. (B) The first derivative of the mag-fluo-4 traces within the region marked by two arrows for the traces shown in A. (C) Box plot representation for the dataset of peak electrically evoked mag-fluo-4 transients ($\Delta F/F_{max}$) in FDB fibers from WT (left) and IT/+ (right) mice. (D) Box plot representation for the dataset for the peak of the first derivative of electrically evoked mag-fluo-4 transients ($d(\Delta F/F)/dt$) in FDB fibers from WT (left) and IT/+ (right) mice. (E) Average (±SEM) peak electrically evoked Ca^{2+} transients ($\Delta F/F_{max}$) across FDB fibers from WT ($n = 3$; black bar) and IT/+ ($n = 3$; gray bar) mice (12–29 fibers/mouse). (F) Mean (±SEM) peak of the first derivative ($d(\Delta F/F)/dt$) across FDB fibers from WT ($n = 3$; black bar) and IT/+ ($n = 3$; gray bar) mice (12–29 fibers/mouse).

intracellular buffer concentration (Schuhmeier and Melzer, 2004). However, the difference in fitted release flux amplitude between WT and IT/+ fibers reached significance when using a single set of removal parameters determined by averaging the values from the individual fibers. At +50 mV, mean peak values were 102 ± 19 for WT and 58 ± 8.4 for IT/+. The Ca^{2+} release flux showed the usual rapid decrease to a slower declining plateau phase after the initial maximum. To quantify these characteristics, we compared the peak/plateau ratio in the WT and IT/+ fibers (plateau measured as the mean flux between 25 and 75 ms after the onset of the pulse). The ratio showed no significant difference. It rose almost linearly between −30 and +50 mV from 2.15 ± 0.47 (WT) and 2.02 ± 0.17 (IT/+) to 7.68 ± 0.72 (WT) and 8.56 ± 0.71 (IT/+).

An increase in release channel sensitivity to activation to both endogenous (e.g., DHPR voltage sensor) and exogenous (e.g., caffeine) triggers is a fundamental property of RYR1 MH and CCD mutations that operate via enhanced Ca^{2+} leak. In our experiments, the voltage sensitivity of the Ca^{2+} transients (Fig. 5 C) obtained in WT and IT/+ fibers was not significantly different. Fig. 5 D shows the normalized peak Ca^{2+} release flux at the different test voltages. Again, no significant difference in the voltage dependence was observed. Thus, unlike the dramatic increase in RYR1 sensitivity to activation by caffeine (Chelu et al., 2006) and voltage (Andronache et al., 2009) observed in muscle fibers from *Ryr1*$^{Y524S/+}$ MH knock-in mice (YS/+), RYR1 Ca^{2+} release channel sensitivity to activation by caffeine (Fig. S1) and voltage (Fig. 5 D) was not enhanced (caffeine sensitivity is actually reduced) in fibers derived from IT/+ mice.

The IT mutation reduces RYR1 channel Ca^{2+} ion permeation

To characterize the mechanism by which IT mutation reduces the magnitude and rate of RYR1 Ca^{2+} release, we used the planar lipid bilayer method to determine the impact of the mutation on RYR1 channel Ca^{2+} conductance and selectivity. For these experiments, HEK293 cells were transfected with WT and IT mutant cDNA (using a rabbit RYR1 cDNA with or without the analogous I4897T mutation) alone or cotransfected at ratios of 2:1, 1:1, and 1:2. Purified channel complexes were incorporated in lipid bilayers and recorded under symmetric 0.25 M KCl and 20 mM HEPES, pH 7.4, conditions with 2 µM of free Ca^{2+} in the cis solution before

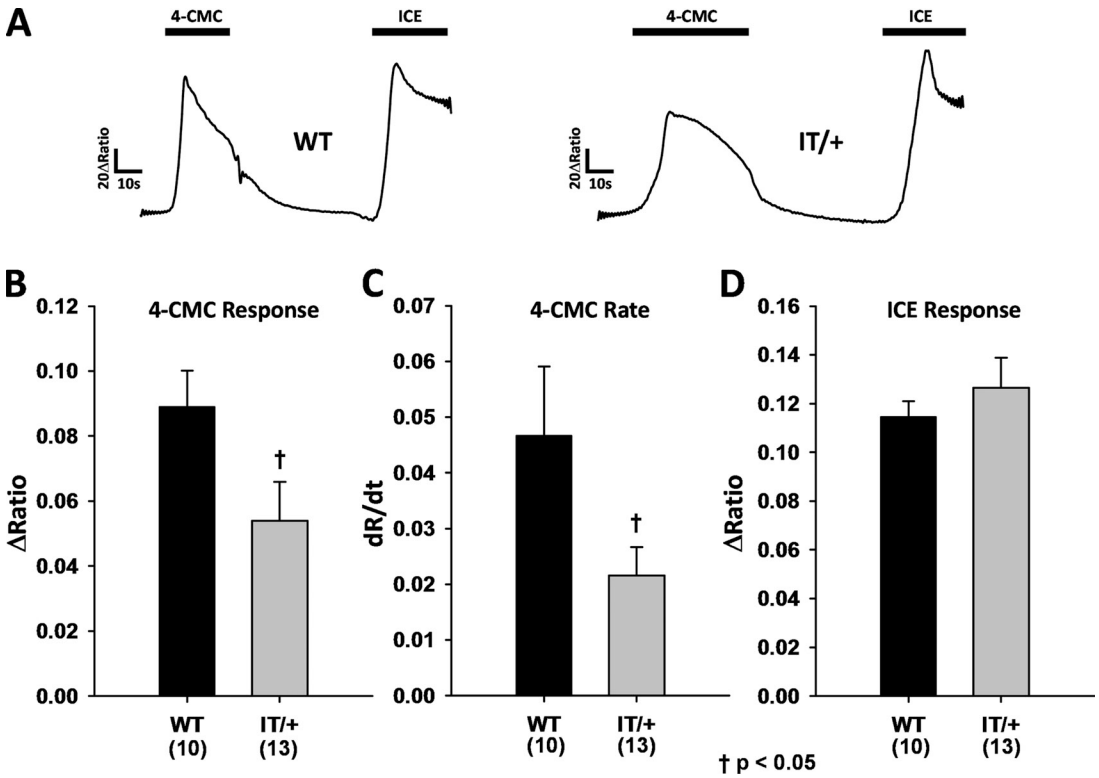

Figure 4. Intracellular Ca^{2+} store content is similar in FDB fibers from WT and IT/+ mice. (A) Representative Fura-FF traces in FDB fibers from WT and IT/+ mice during successive applications of 500 µM 4-CMC and ICE (10 µM ionomycin, 30 µM CPA, and 100 µM EGTA/0 Ca^{2+} Ringer's solution). (B) Average (±SEM) peak Fura-FF responses to 4-CMC in FDB fibers from WT (n = 10; left) and IT/+ (n = 13; right) mice. (C) Average (±SEM) peak rate of change in Fura-FF ratio (F_{340}/F_{380}) during 4-CMC application in FDB fibers from WT (n = 10; left) and IT/+ (n = 13; right) mice. (D) Average (±SEM) peak ICE responses in FDB fibers from WT (n = 10; left) and IT/+ (n = 13; right) mice. †, $P < 0.05$.

and after the addition of 10 mM Ca^{2+} to the trans (SR luminal) bilayer chamber. In Fig. 6, WT and mutant cDNAs were cotransfected at ratio of 1:1. Fig. 6 A shows a representative set of single channels recorded at −35 mV (left traces) and 0 mV (right traces) before and after the addition of the 10 mM Ca^{2+}, respectively. In WT:IT coexpression preparations, we detected three groups of single channels that differed in their ion permeability properties. Group 1 (six channels) had single-channel properties identical to WT expressed alone, and Group 3 (nine channels) had properties identical to I4897T expressed alone. Group 1 channels exhibited a well-defined K^+ conductance (795 ± 10 pS) and conducted a significant Ca^{2+} current at 0 mV (i_{Ca} = −2.4 ± 0.1 pA), whereas Group 3 channels showed a more variable K^+ conductance (268 ± 42 pS) among the preparations and essentially lost the ability to conduct Ca^{2+} (Table I). One additional group of single channels (Group 2; five channels) was detected when WT and I4897T were coexpressed. Group 2 channels had a K^+ conductance comparable to WT (795 ± 10 pS and 790 ± 5 pS for Group 1 and Group 2 channels, respectively) but exhibited a significantly ($P < 0.05$) lower Ca^{2+} current at 0 mV (I_{Ca} was −2.4 ± 0.1 pA and −2.1 ± 0.1 pA for Group 1 and Group 2 channels, respectively). In addition, Group 2 channels displayed a less positive reversal potential compared with WT (E_{rev} was 9.2 ± 0.2 mV and 7.2 ± 0.2 mV for Group 1 and Group 2 channels, respectively) from which, applying constant field theory, resulted in a reduced calculated permeability ratio of Ca^{2+} over K^+ (P_{Ca}/P_K was 6.8 ± 0.2 and 4.8 ± 0.1 for Group 1 and Group 2 channels, respectively). Compared with Group 1 channels, average i_{Ca}, E_{rev}, and P_{Ca}/P_K values were all significantly ($P < 0.05$) reduced for Group 2 channels (Table I). Fig. 6 B shows average current–voltage curves for Group 1 and Group 2 channels recorded in the presence of 10 mM of luminal Ca^{2+} at voltages. The modest reduction in i_{Ca} magnitude at 0 mV and the less positive E_{rev} of Group 2 channels are best illustrated in Fig. 6 C, which plots an expanded view of the data within the boxed region of Fig. 6 B. Out of 20 channels examined from proteoliposomes derived from the coexpression of WT and IT subunits, 9 were found to be Group 3 channels (i.e., conduct K^+ ions but do not conduct Ca^{2+} ions). Also, the observed frequency of Group 3 channels in the bilayer experiments (9/20) is much higher than the expected frequency of homotypic IT:IT channels, assuming an independent assortment of WT and IT subunits (1/16). Given the experimentally observed frequency of Group 1, 2, and 3 channels in our bilayer experiments (6:5:9, respectively), we postulate that Group 1 channels arise from tetramers with only one or fewer IT subunits, Group 2 channels from tetramers with two WT and two IT subunits, and Group 3 channels from tetramers with three or more IT subunits (Fig. 6 D, left). Given this distribution, the model predicts an overall 36% net reduction in RYR1 fractional Ca conductance (Fig. 6 D, right), which correlates remarkably well with the reduction

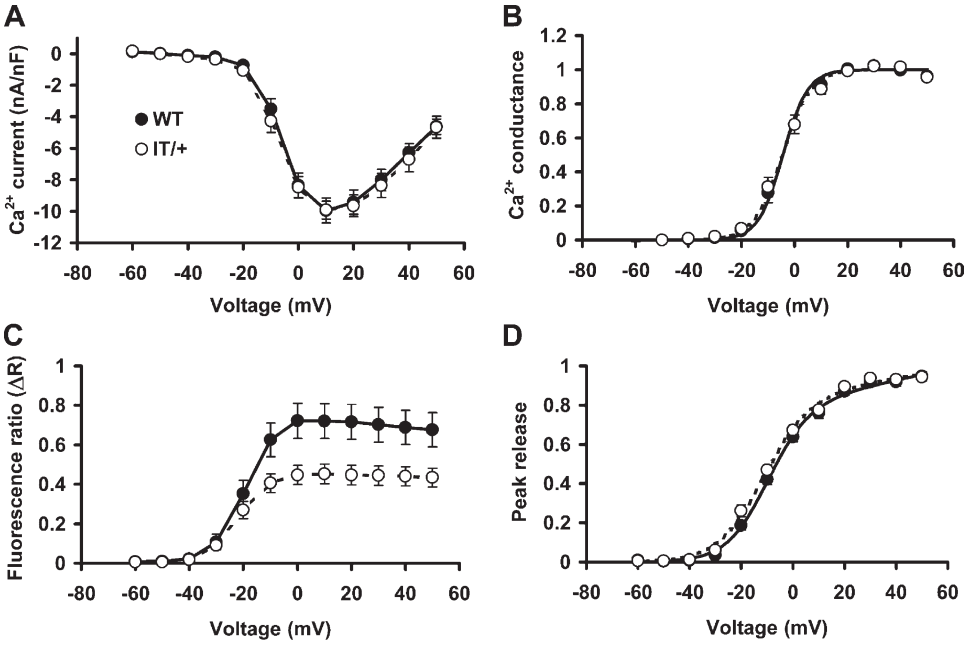

Figure 5. L-type Ca^{2+} currents and SR Ca^{2+} release flux in muscle fibers from WT and IT/+ mice. (A) Voltage dependence of L-type Ca^{2+} current density. (B) Normalized Ca^{2+} conductance derived from the data shown in A ($V_{1/2}$, k, and G_{max} were −4.38 ± 1.58 mV, 4.66 ± 0.28 mV, and 154 ± 14.6 SF^{-1} for WT and −4.57 ± 1.41 mV, 5.33 ± 0.20 mV, and 162 ± 15.3 SF^{-1} for IT/+, respectively). Mean membrane capacitance was 5.06 ± 0.25 nF (WT) and 4.72 ± 0.38 nF (IT/+). (C) Voltage-activated changes in fura-2 fluorescence ratio. All mean values above −20 mV were significantly ($P < 0.05$) different, in contrast to the parameters $V_{1/2}$ and k, which were not significantly different (−18.5 ± 1.29 mV and 5.15 ± 0.24 mV for WT and −21.6 ± 1.24 mV and 5.17 ± 0.30 mV for IT/+, respectively). (D) Normalized peak Ca^{2+} release flux. Values from the different experiments were averaged after normalization to the maximum. $V_{1/2}$ and k were not significantly different (−10.0 ± 1.9 mV and 7.54 ± 0.56 mV for WT and −12.2 ± 1.19 mV and 8.54 ± 0.46 mV for IT/+, respectively). The absolute maximal values (assuming internal EGTA concentration to be 40% of the pipette concentration) at +50 mV were 64.6 ± 17.5 and 49.9 ± 9.4 mM/s, respectively. Current and fluorescence signals were simultaneously recorded in isolated interosseus fibers (WT, filled circles and continuous lines, $n = 15$; IT/+, open circles and dashed lines, $n = 14$).

in the global Ca transient observed during EC coupling in fibers from IT/+ mice (Figs. 2 B, 3, and 5 C).

Osmotic shock–induced ECREs in fibers from IT/+ mice

Measuring ECREs provides an alternative method to assess RYR1 Ca^{2+} release channel function within the context of a minimally altered intracellular muscle environment. In adult mammalian skeletal muscle fibers, ECREs can be induced by osmotic alterations of the bathing solution (Wang et al., 2005). Therefore, in additional experiments, we used a hyperosmotic shock paradigm to compare ECRE properties as an index of RYR1-mediated SR Ca^{2+} release in single intact muscle fibers of WT and IT/+ mice (Fig. S2, A and B). Statistical evaluation of all assessed ECRE parameters (frequency, FDHM, FWHM, amplitude, and event mass) showed significant differences in fibers from IT/+ mice, although the extent of the fractional changes was largest for frequency (Fig. S2 C). Specifically, mean ECRE frequency was significantly reduced by 56% ($P < 0.05$), and signal mass, a measure of net Ca^{2+} flux during a release event (Hollingworth et al., 2001), was significantly reduced by 21% ($P < 0.01$) in fibers from IT/+ mice. These results are consistent with an overall reduction in osmotic shock–induced RYR1 Ca^{2+} release.

DISCUSSION

Heterozygous *Ryr1*^{I4895T} knock-in mice (IT/+) provide a powerful animal model for the systematic evaluation of the effects of endogenous expression of a common

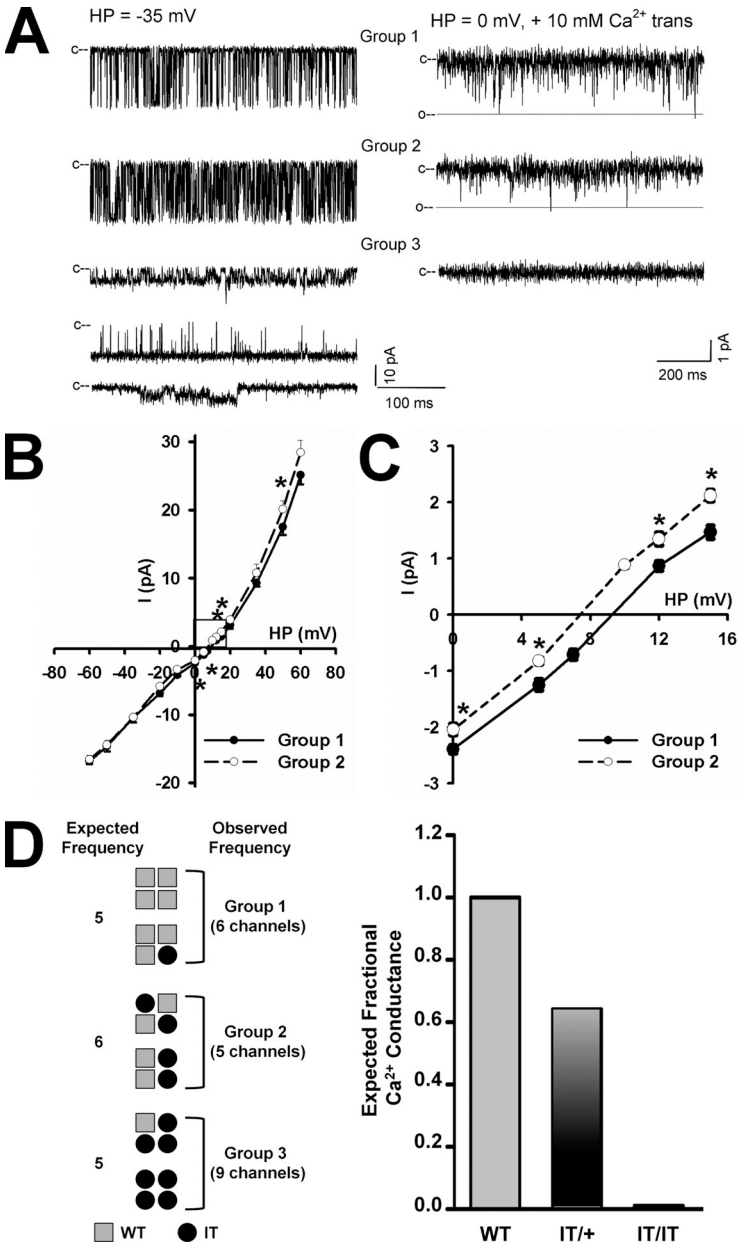

Figure 6. Single-channel recordings of coexpressed WT and IT channels . (A) Representative single-channel currents were recorded at −35 mV (left traces) or 0 mV (right traces), with openings represented by downward deflections from the closed state (c–) in symmetrical 250 mM KCl and 2 µM cis Ca^{2+} (left traces) and after the subsequent addition of 10 mM trans Ca^{2+} (right traces). Three traces of Group 3 channels recorded in the absence of 10 mM trans Ca^{2+} (left) indicate the absence of well-defined K^+ conductance. Group 3 channels lack a Ca^{2+} current at 0 mV in the presence of 10 mM trans Ca^{2+}. (B) Current–voltage relationships of Group 1 (●) and Group 2 (○) channels in 250 mM of symmetric KCl plus 10 mM trans Ca^{2+}. (C) The boxed region indicated in B is expanded to highlight the negative shift in the reversal potential of Group 2 channels. (D) Proposed tetramer assembly model based on the assumption of independent WT and IT subunit assortment (left) and the expected reduction in fractional RYR1 Ca^{2+} conductance in muscle cells obtained from IT/+ and IT/IT mice (right), provided that Group 1 channels arise from tetramers with only one or fewer IT subunits, Group 2 channels from tetramers with two WT and two IT subunits, and Group 3 channels from tetramers with three or more IT subunits.

TABLE I

Activities and unitary properties of coexpressed WT and IT Channels

Property	Group 1[a]	Group 2[a]	Group 3[a]
P_o	0.28 ± 0.07 (6)	0.30 ± 0.10 (5)	ND
No. of events/min	17,411 ± 4,948	19,327 ± 6,392	ND
T_o (ms)	0.55 ± 0.09	0.55 ± 0.10	ND
T_c (ms)	1.93 ± 0.49	2.56 ± 1.10	ND
K^+ conductance (pS)	799 ± 10 (6)	790 ± 5 (5)	269 ± 42[b] (9)
I_{Ca}^{2+} at 0 mV (pA)	−2.4 ± 0.1	−2.1 ± 0.1[b]	<0.1[b]
E_{rev} (mV)	9.2 ± 0.2	7.2 ± 0.1[b]	ND
P_{Ca}/P_K	6.8 ± 0.2	4.8 ± 0.1[b]	ND

The number in parenthesis indicates the number of determinations. ND, not determined.

[a]See Fig. 6 D for proposed tetramer composition of Group 1–3 channels.

[b]$P < 0.05$ compared to WT.

CCD mutation in the RYR1 pore region on skeletal muscle performance and Ca^{2+} handling in fully differentiated adult muscle fibers. Using this model, we compared in vivo upper body and grip strength of WT and IT/+ knock-in mice and also assessed bidirectional DHPR–RYR1 conformational coupling, RYR1-mediated Ca^{2+} release, and intracellular Ca^{2+} store content in single muscle fibers from these mice. Consistent with the decrease in twitch contraction and rate of force development reported previously (Zvaritch et al., 2009), IT/+ mice exhibited a significant reduction in upper body and grip strength (Fig. 1). Single skeletal muscle fibers from IT/+ mice exhibited a significant reduction in both the magnitude and maximum rate of RYR1-mediated Ca^{2+} release during EC coupling (Figs. 2 and 3) and 4-CMC–induced activation (Figs. 2 and 4) that occurred in the absence of a change in intracellular Ca^{2+} store content (Fig. 4) or increased sensitivity to activation by voltage (Fig. 5) or caffeine (Fig. S1). Analysis of osmotic shock–induced ECREs revealed a significantly reduced frequency and signal mass in fibers from IT/+ mice (Fig. S2). Finally, using purified recombinant channels incorporated into planar lipid bilayers, we demonstrate that the incorporation of IT mutant subunits into the RYR1 tetramer results in significant reductions in RYR1 channel Ca^{2+} conductance and P_{Ca}/P_K (Fig. 6 and Table I). Collectively, these findings indicate that the in vivo muscle weakness of IT/+ knock-in mice arises in part from a reduction in the magnitude and rate of RYR1 Ca^{2+} release during EC coupling as a result of the incorporation of IT subunits into release channel tetramers, which results in a dominant-negative suppression of RYR1 channel Ca^{2+} conduction.

The IT mutation alters RYR1 Ca^{2+} release by reducing Ca^{2+} ion permeation

The position of the I4895T mutation lies within the center of the selectivity filter of the RYR1 Ca^{2+} release channel (Balshaw et al., 1999; Zhao et al., 1999). Given its location, mutations of this residue could conceivably either enhance or reduce Ca^{2+} conductance and selectivity. Previous studies of recombinant channels incorporated into lipid bilayers demonstrated that mutations of residues within the RYR1 pore region decrease RYR channel ion selectivity and conduction (Zhao et al., 1999; Gao et al., 2000). Specifically, conservative mutations of Ile^{4895} to Ala, Leu, or Val resulted in marked reductions in RYR1 single-channel conductance and Ca^{2+} selectivity (Gao et al., 2000). Subsequent studies of RYR1 mutations linked to CCD (G4898E, G4898R, and ΔV4926/I4927) and multi-minicore disease (R110W/L486V) were all shown to exhibit negligible Ca^{2+} permeation, loss of Ca^{2+}-dependent channel activity, and reduced K^+ conductance (Xu et al., 2008). Coexpression of WT and mutant RYR1s resulted in three groups of channels that exhibited different permeability ratios of Ca^{2+} over K^+, consistent with heterotetrameric RYR1 complexes composed of WT and mutant subunits. The number of WT subunits required to maintain a functional heterotetrameric channel differed among the four RYR1 mutants. K^+ conductances comparable to WT were predicted to require the presence of three (R110W/L486V), two (ΔV4926/I4927), or only one (G4898E and G4898R) WT subunit. Here, we demonstrate that RYR1 Ca^{2+} conduction and gating are abolished in homotetrameric IT channels. Although the precise effect of the IT mutation on the structure of the RYR1 channel is unknown, the observed alterations in Ca^{2+} gating and conductance of homomeric and heteromeric IT channels are similar to those observed previously for other CCD mutations located within the RYR1 selectivity filter (Xu et al., 2008). Only one group of channels with a modestly reduced Ca^{2+} conductance and selectivity was observed in single-channel recordings when WT and IT channels were coexpressed (Group 2 channels). Assuming independent assortment of subunits according to a binomial distribution (1:4:6:4:1), and given the similar number of Group 1 (six channels), Group 2 (five channels), and Group 3 (nine channels) single channels recorded from the coexpression experiments, our results can best be rationalized by Group 2 channels exhibiting two mutant and two WT subunits. In this case, the presence of fewer than two mutant channels would result in Group 1 (channels with WT:WT properties) channels and more than two mutant subunits would result in Group 3 (channels IT:IT properties) channels (Fig. 6 D, left). Consistent with these findings, depolarization- and 4-CMC–induced Ca^{2+} release is absent whereas SR Ca^{2+} content is unaltered in myotubes from homozygous IT/IT mice (Zvaritch et al., 2007), and the magnitude and rate of SR Ca^{2+} release are reduced in muscle fibers from heterozygous adult IT/+ mice (Figs. 2–5). Specifically, the overall weighted impact of the three observed channel types on Ca^{2+} conduction (Group 1 being normal, Group 2 being reduced ∼12.5%, and Group 3 being reduced ∼100%) would be predicted to decrease

maximal global Ca release by ∼36% (Fig. 6 D, right), which is remarkably similar to that reported in Figs. 2–5. Thus, the observed deficits in in vivo muscle performance in 4–6-mo-old IT/+ mice arises, at least in part, from a reduction in SR Ca^{2+} release as a result of the aggregate effect of the formation of Group 2 and Group 3 RYR1 release channels that exhibit deficits in Ca^{2+} ion conduction.

EC uncoupling in muscle fibers from I4895T/+ knock-in mice

The human *RYR1*^{I4898T} CCD mutation (mouse, *Ryr1*^{I4895T}) was the first RYR1 disease mutation identified in the C-terminal transmembrane region of the channel (Lynch et al., 1999). Subsequent studies indicate that the majority (>60%) of CCD mutations in RYR1 are located in the C-terminal one fifth of the protein (Robinson et al., 2006; Rosenberg et al., 2010). Lynch et al. (1999) reported that muscle biopsies from two affected individuals revealed type I fiber predominance and central cores in >50–85% of fibers. On the basis of increased resting Ca^{2+} levels measured in HEK293 cells in which the heterozygous rabbit I4897T mutant cDNA was coexpressed with SERCA1a, this study concluded that the mutation enhances RYR1-mediated Ca^{2+} leak. A similar conclusion was reached based on experiments conducted in B lymphocytes (Tilgen et al., 2001) and human myotubes (Ducreux et al., 2004) derived from patients heterozygous for the I4898T mutation.

In contrast, results obtained after homologous expression of the mutant alone in dyspedic myotubes (Avila et al., 2001) and from myotubes derived from homozygous IT/IT knock-in mice (Zvaritch et al., 2007) showed a complete loss of RYR1 Ca^{2+} release in response to depolarization and pharmacological activation of homotetrameric IT/IT channels, despite normal levels of SR Ca^{2+} content. These prior results, coupled with our findings that the IT mutation reduces RYR1 Ca^{2+} permeation (Fig. 6 and Table I) without significantly altering SR Ca^{2+} content (Fig. 4), suggest that resting WT RYR1 Ca^{2+} leak is low enough that basal SR Ca^{2+} reuptake mechanisms are sufficient to maintain a full SR Ca^{2+} store complement. We have referred to the process by which RYR1 mutations reduce depolarization-induced Ca^{2+} release in the absence of increased SR Ca^{2+} leak, Ca^{2+} store depletion, or sensitization of the channel to activation as "EC uncoupling" (Avila and Dirksen, 2001; Avila et al., 2001, 2003). Theoretically, EC uncoupling could result from several distinct mechanisms, including reduced RYR1 expression, lack of appropriate RYR1 junctional targeting, defective coupling to the DHPR, or altered RYR1 Ca^{2+} conduction and/or gating. Here, we demonstrate that single adult fibers from IT/+ knock-in mice exhibit significantly reduced and slowed RYR1 Ca^{2+} release in the absence of a change in either SR Ca^{2+} content or release channel sensitivity to voltage and caffeine activation (EC uncoupling). Moreover, we provide evidence that the mechanism of EC uncoupling observed in muscle from IT/+ mice results from the formation of heterotetrameric RYR1 channels with reduced Ca^{2+} ion permeation.

It is not entirely clear whether the IT/+ mutation in the RYR1 pore region leads to MH susceptibility in humans. Lynch et al. (1999) reported that muscle biopsies from two affected individuals exhibited positive responses to standardized in vitro contracture tests (IVCTs) for MH susceptibility. However, no anesthetic complications were observed in this family, despite the exposure of 19 affected members to MH-triggering agents. Subsequently, six other kindreds positive for the *RYR1*^{I4898T} mutation have been identified, and no anesthetic complications have been reported in these families. Understandably, costly and invasive diagnostic IVCT analyses of muscle biopsies have not been conducted in these families. Because some patients with muscular disorders unrelated to MH are known to test positive at times with the IVCT (Iaizzo and Lehmann-Horn, 1995; Shepherd et al., 2004), the positive IVCT results reported by Lynch et al. (1999) could reflect the presence of an underlying myopathy rather than a genuine increased susceptibility to MH. Here, we found that SR Ca^{2+} release channels in adult fibers from IT/+ mice do not exhibit increased sensitivity to activation by either voltage (Fig. 5) or caffeine (Fig. S1). These findings suggest that the IT/+ genotype is unlikely to predispose an individual to an MH episode during either heat challenge or exposure to MH-triggering anesthetic agents, as is seen in *Ryr1*$^{Y524S/+}$ (YS/+) (Chelu et al., 2006) and *Ryr1*$^{R163C/+}$ (Yang et al., 2006) knock-in mice that possess mutations known to increase RYR1 Ca^{2+} leak. Consistent with this suggestion, we have found that IT/+ mice do not experience lethal hypermetabolic episodes after exposure to heat stress (unpublished data).

Implications of EC uncoupling for the progression of structural alterations in skeletal muscle of IT/+ mice

Recent studies have characterized the time-dependent development of skeletal muscle morphological abnormalities during the ∼2-year lifespan of IT/+ (Zvaritch et al., 2009; Boncompagni et al., 2010) and YS/+ (Durham et al., 2008; Boncompagni et al., 2009) knock-in mice. At the ultrastructural level, the mutations result in two very distinct pathologies. In IT/+ mice, muscle fibers undergo an age-dependent progression, with Zvaritch et al. (2009) reporting 7% of fibers showing significant structural abnormalities at 6 wk, 14% at 6 mo, and 65% at 18 mo of age. Some aged IT/+ mice examined by Zvaritch et al. (2009) displayed an overt skeletal muscle phenotype, including the presence of minicores, cores, and nemaline rods. Throughout this progression, although mitochondria were displaced within regions of structural disorganization, they did not show

signs of swelling or degeneration. A more benign age-dependent morphological phenotype was observed in IT/+ mice from our colony (Boncompagni et al., 2010). Nevertheless, functional findings in 4–6-mo-old IT/+ mice presented here indicate that the EC uncoupling defect manifests early within this temporal spectrum, preceding the development of major structural alterations.

In dramatic contrast to that observed in IT/+ mice, skeletal muscle from YS/+ mice that express a mutation that enhances RYR1 Ca^{2+} leak and results in MH susceptibility develops localized regions of mitochondrial and sarcotubular disruption observed as early as 2 mo postnatal (Boncompagni et al., 2009). In these focal regions of disruption, mitochondria are swollen, present a more translucent matrix, and exhibit significant cristae remodeling. At somewhat later stages, between 3 and 12 mo of age, these regions become larger and exhibit contracted myofibrils that lack SR and mitochondria. By 1 year of age, these "contraction cores" progress to larger unstructured cores that also lack contractile elements, SR, and mitochondria (Boncompagni et al., 2009). Collectively, the marked difference in the functional and structural characteristics of skeletal muscle from IT/+ and YS/+ knock-in mice provide compelling evidence that the two mutations indeed operate via fundamentally distinct mechanisms (i.e., EC uncoupling and enhanced RYR1 Ca^{2+} leak).

Summary

Our studies using IT/+ knock-in mice provide strong evidence that the I4895T mutation in the RYR1 selectivity filter: (a) reduces RYR1 channel Ca^{2+} ion permeation in a manner that leads to a parallel reduction in both the magnitude and rate of RYR1-mediated Ca^{2+} release during EC coupling or ligand activation; (b) does not significantly alter either RYR1 Ca^{2+} leak, SR Ca^{2+} store content, or RYR1 channel sensitivity to activation by either voltage or caffeine; and (c) is unlikely to predispose an individual to MH susceptibility.

We thank Professor F. Lehmann-Horn for providing access to the confocal microscope used in this study, Drs. D. Ursu and R.P. Schuhmeier for writing analysis software, Drs. K. Fuchs and A. Riecker for expert technical help, and Dr. T. Begenisich for numerous enlightening and helpful discussions during the course of this project.

This work was supported by research grants from the National Institutes of Health (AR044657 and AR053349 to R.T. Dirksen and AR018687 to G. Meissner), the Canadian Institutes of Health Research (MT 3399 and MOP 49493 to D.H. MacLennan), the Deutsche Forschungsgemeinschaft (ME-713/18 to W. Melzer), and a National Institutes of Health Dental and Craniofacial Training Grant (T32DE07202 to R.E. Loy).

Edward N. Pugh Jr. served as editor.

Submitted: 24 August 2010
Accepted: 17 November 2010

REFERENCES

Andronache, Z., S.L. Hamilton, R.T. Dirksen, and W. Melzer. 2009. A retrograde signal from RyR1 alters DHP receptor inactivation and limits window Ca^{2+} release in muscle fibers of Y522S RyR1 knock-in mice. *Proc. Natl. Acad. Sci. USA.* 106:4531–4536. doi:10.1073/pnas.0812661106

Apostol, S., D. Ursu, F. Lehmann-Horn, and W. Melzer. 2009. Local calcium signals induced by hyper-osmotic stress in mammalian skeletal muscle cells. *J. Muscle Res. Cell Motil.* 30:97–109. doi:10.1007/s10974-009-9179-8

Avila, G., and R.T. Dirksen. 2000. Functional impact of the ryanodine receptor on the skeletal muscle L-type Ca^{2+} channel. *J. Gen. Physiol.* 115:467–480. doi:10.1085/jgp.115.4.467

Avila, G., and R.T. Dirksen. 2001. Functional effects of central core disease mutations in the cytoplasmic region of the skeletal muscle ryanodine receptor. *J. Gen. Physiol.* 118:277–290. doi:10.1085/jgp.118.3.277

Avila, G., J.J. O'Brien, and R.T. Dirksen. 2001. Excitation–contraction uncoupling by a human central core disease mutation in the ryanodine receptor. *Proc. Natl. Acad. Sci. USA.* 98:4215–4220. doi:10.1073/pnas.071048198

Avila, G., K.M. O'Connell, and R.T. Dirksen. 2003. The pore region of the skeletal muscle ryanodine receptor is a primary locus for excitation–contraction uncoupling in central core disease. *J. Gen. Physiol.* 121:277–286. doi:10.1085/jgp.200308791

Balshaw, D., L. Gao, and G. Meissner. 1999. Luminal loop of the ryanodine receptor: a pore-forming segment? *Proc. Natl. Acad. Sci. USA.* 96:3345–3347. doi:10.1073/pnas.96.7.3345

Beam, K.G., and C.M. Knudson. 1988. Calcium currents in embryonic and neonatal mammalian skeletal muscle. *J. Gen. Physiol.* 91:781–798. doi:10.1085/jgp.91.6.781

Block, B.A., T. Imagawa, K.P. Campbell, and C. Franzini-Armstrong. 1988. Structural evidence for direct interaction between the molecular components of the transverse tubule/sarcoplasmic reticulum junction in skeletal muscle. *J. Cell Biol.* 107:2587–2600. doi:10.1083/jcb.107.6.2587

Boncompagni, S., A.E. Rossi, M. Micaroni, S.L. Hamilton, R.T. Dirksen, C. Franzini-Armstrong, and F. Protasi. 2009. Characterization and temporal development of cores in a mouse model of malignant hyperthermia. *Proc. Natl. Acad. Sci. USA.* 106:21996–22001.

Boncompagni, S., R.E. Loy, R.T. Dirksen, and C. Franzini-Armstrong. 2010. The I4895T mutation in the type 1 ryanodine receptor induces fiber-type specific alterations in skeletal muscle that mimic premature aging. *Aging Cell.* 9:958–970. doi:10.1111/j.1474-9726.2010.00623.x

Brooks, S.P., and S.B. Dunnett. 2009. Tests to assess motor phenotype in mice: a user's guide. *Nat. Rev. Neurosci.* 10:519–529. doi:10.1038/nrn2652

Capote, J., P. Bolaños, R.P. Schuhmeier, W. Melzer, and C. Caputo. 2005. Calcium transients in developing mouse skeletal muscle fibres. *J. Physiol.* 564:451–464. doi:10.1113/jphysiol.2004.081034

Chelu, M.G., S.A. Goonasekera, W.J. Durham, W. Tang, J.D. Lueck, J. Riehl, I.N. Pessah, P. Zhang, M.B. Bhattacharjee, R.T. Dirksen, and S.L. Hamilton. 2006. Heat- and anesthesia-induced malignant hyperthermia in an RyR1 knock-in mouse. *FASEB J.* 20:329–330.

Dainese, M., M. Quarta, A.D. Lyfenko, C. Paolini, M. Canato, C. Reggiani, R.T. Dirksen, and F. Protasi. 2009. Anesthetic- and heat-induced sudden death in calsequestrin-1-knockout mice. *FASEB J.* 23:1710–1720. doi:10.1096/fj.08-121335

Dirksen, R.T. 2002. Bi-directional coupling between dihydropyridine receptors and ryanodine receptors. *Front. Biosci.* 7:d659–d670. doi:10.2741/dirksen

Dirksen, R.T., and G. Avila. 2002. Altered ryanodine receptor function in central core disease: leaky or uncoupled $Ca^{(2+)}$

release channels? *Trends Cardiovasc. Med.* 12:189–197. doi:10.1016/S1050-1738(02)00163-9

Dirksen, R.T., and G. Avila. 2004. Distinct effects on Ca^{2+} handling caused by malignant hyperthermia and central core disease mutations in RyR1. *Biophys. J.* 87:3193–3204. doi:10.1529/biophysj.104.048447

Du, G.G., B. Sandhu, V.K. Khanna, X.H. Guo, and D.H. MacLennan. 2002. Topology of the Ca^{2+} release channel of skeletal muscle sarcoplasmic reticulum (RyR1). *Proc. Natl. Acad. Sci. USA.* 99:16725–16730. doi:10.1073/pnas.012688999

Du, G.G., G. Avila, P. Sharma, V.K. Khanna, R.T. Dirksen, and D.H. MacLennan. 2004. Role of the sequence surrounding predicted transmembrane helix M4 in membrane association and function of the Ca($^{2+}$) release channel of skeletal muscle sarcoplasmic reticulum (ryanodine receptor isoform 1). *J. Biol. Chem.* 279:37566–37574. doi:10.1074/jbc.M406637200

Ducreux, S., F. Zorzato, C. Müller, C. Sewry, F. Muntoni, R. Quinlivan, G. Restagno, T. Girard, and S. Treves. 2004. Effect of ryanodine receptor mutations on interleukin-6 release and intracellular calcium homeostasis in human myotubes from malignant hyperthermia-susceptible individuals and patients affected by central core disease. *J. Biol. Chem.* 279:43838–43846. doi:10.1074/jbc.M403612200

Durham, W.J., P. Aracena-Parks, C. Long, A.E. Rossi, S.A. Goonasekera, S. Boncompagni, D.L. Galvan, C.P. Gilman, M.R. Baker, N. Shirokova, et al. 2008. RyR1 S-nitrosylation underlies environmental heat stroke and sudden death in Y522S RyR1 knockin mice. *Cell.* 133:53–65. doi:10.1016/j.cell.2008.02.042

Franzini-Armstrong, C., and J.W. Kish. 1995. Alternate disposition of tetrads in peripheral couplings of skeletal muscle. *J. Muscle Res. Cell Motil.* 16:319–324. doi:10.1007/BF00121140

Franzini-Armstrong, C., and G. Nunzi. 1983. Junctional feet and particles in the triads of a fast-twitch muscle fibre. *J. Muscle Res. Cell Motil.* 4:233–252. doi:10.1007/BF00712033

Gao, L., D. Balshaw, L. Xu, A. Tripathy, C. Xin, and G. Meissner. 2000. Evidence for a role of the lumenal M3-M4 loop in skeletal muscle Ca($^{2+}$) release channel (ryanodine receptor) activity and conductance. *Biophys. J.* 79:828–840. doi:10.1016/S0006-3495(00)76339-9

Hollingworth, S., J. Peet, W.K. Chandler, and S.M. Baylor. 2001. Calcium sparks in intact skeletal muscle fibers of the frog. *J. Gen. Physiol.* 118:653–678. doi:10.1085/jgp.118.6.653

Iaizzo, P.A., and F. Lehmann-Horn. 1995. Anesthetic complications in muscle disorders. *Anesthesiology.* 82:1093–1096. doi:10.1097/00000542-199505000-00001

Jiang, D., W. Chen, J. Xiao, R. Wang, H. Kong, P.P. Jones, L. Zhang, B. Fruen, and S.R. Chen. 2008. Reduced threshold for luminal Ca^{2+} activation of RyR1 underlies a causal mechanism of porcine malignant hyperthermia. *J. Biol. Chem.* 283:20813–20820. doi:10.1074/jbc.M801944200

Jungbluth, H., H. Zhou, L. Hartley, B. Halliger-Keller, S. Messina, C. Longman, M. Brockington, S.A. Robb, V. Straub, T. Voit, et al. 2005. Minicore myopathy with ophthalmoplegia caused by mutations in the ryanodine receptor type 1 gene. *Neurology.* 65:1930–1935. doi:10.1212/01.wnl.0000188870.37076.f2

Jungbluth, H., H. Zhou, C.A. Sewry, S. Robb, S. Treves, M. Bitoun, P. Guicheney, A. Buj-Bello, C. Bönnemann, and F. Muntoni. 2007. Centronuclear myopathy due to a de novo dominant mutation in the skeletal muscle ryanodine receptor (RYR1) gene. *Neuromuscul. Disord.* 17:338–345. doi:10.1016/j.nmd.2007.01.016

Kimura, T., J.D. Lueck, P.J. Harvey, S.M. Pace, N. Ikemoto, M.G. Casarotto, R.T. Dirksen, and A.F. Dulhunty. 2009. Alternative splicing of RyR1 alters the efficacy of skeletal EC coupling. *Cell Calcium.* 45:264–274. doi:10.1016/j.ceca.2008.11.005

Lynch, P.J., J. Tong, M. Lehane, A. Mallet, L. Giblin, J.J. Heffron, P. Vaughan, G. Zafra, D.H. MacLennan, and T.V. McCarthy. 1999. A mutation in the transmembrane/luminal domain of the ryanodine receptor is associated with abnormal Ca^{2+} release channel function and severe central core disease. *Proc. Natl. Acad. Sci. USA.* 96:4164–4169. doi:10.1073/pnas.96.7.4164

Matsuo, N., K. Tanda, K. Nakanishi, N. Yamasaki, K. Toyama, K. Takao, H. Takeshima, and T. Miyakawa. 2009. Comprehensive behavioral phenotyping of ryanodine receptor type 3 (RyR3) knockout mice: decreased social contact duration in two social interaction tests. *Front Behav Neurosci.* 3:3.

Melzer, W., E. Ríos, and M.F. Schneider. 1986. The removal of myoplasmic free calcium following calcium release in frog skeletal muscle. *J. Physiol.* 372:261–292.

Mickelson, J.R., and C.F. Louis. 1996. Malignant hyperthermia: excitation-contraction coupling, Ca^{2+} release channel, and cell Ca^{2+} regulation defects. *Physiol. Rev.* 76:537–592.

Monnier, N., V. Procaccio, P. Stieglitz, and J. Lunardi. 1997. Malignant-hyperthermia susceptibility is associated with a mutation of the alpha 1-subunit of the human dihydropyridine-sensitive L-type voltage-dependent calcium-channel receptor in skeletal muscle. *Am. J. Hum. Genet.* 60:1316–1325. doi:10.1086/515454

Monnier, N., A. Ferreiro, I. Marty, A. Labarre-Vila, P. Mezin, and J. Lunardi. 2003. A homozygous splicing mutation causing a depletion of skeletal muscle RYR1 is associated with multi-minicore disease congenital myopathy with ophthalmoplegia. *Hum. Mol. Genet.* 12:1171–1178. doi:10.1093/hmg/ddg121

Murayama, T., T. Oba, H. Hara, K. Wakebe, N. Ikemoto, and Y. Ogawa. 2007. Postulated role of interdomain interaction between regions 1 and 2 within type 1 ryanodine receptor in the pathogenesis of porcine malignant hyperthermia. *Biochem. J.* 402:349–357. doi:10.1042/BJ20061040

Nakai, J., R.T. Dirksen, H.T. Nguyen, I.N. Pessah, K.G. Beam, and P.D. Allen. 1996. Enhanced dihydropyridine receptor channel activity in the presence of ryanodine receptor. *Nature.* 380:72–75. doi:10.1038/380072a0

Ogura, H., J. Aruga, and K. Mikoshiba. 2001. Behavioral abnormalities of Zic1 and Zic2 mutant mice: implications as models for human neurological disorders. *Behav. Genet.* 31:317–324. doi:10.1023/A:1012235510600

Protasi, F., C. Franzini-Armstrong, and B.E. Flucher. 1997. Coordinated incorporation of skeletal muscle dihydropyridine receptors and ryanodine receptors in peripheral couplings of BC3H1 cells. *J. Cell Biol.* 137:859–870. doi:10.1083/jcb.137.4.859

Robinson, R., D. Carpenter, M.A. Shaw, J. Halsall, and P. Hopkins. 2006. Mutations in RYR1 in malignant hyperthermia and central core disease. *Hum. Mutat.* 27:977–989. doi:10.1002/humu.20356

Rosenberg, H., N. Sambuughin, and R.T. Dirksen. 2010. Malignant hyperthermia susceptibility. *GeneReviews.* R.A. Pagon, T.C. Bird, C.R. Dolan, and K. Stephens, editors. University of Washington, Seattle. (updated Jan. 19, 2010).

Schuhmeier, R.P., and W. Melzer. 2004. Voltage-dependent Ca^{2+} fluxes in skeletal myotubes determined using a removal model analysis. *J. Gen. Physiol.* 123:33–51. doi:10.1085/jgp.200308908

Shepherd, S., F. Ellis, J. Halsall, P. Hopkins, and R. Robinson. 2004. RYR1 mutations in UK central core disease patients: more than just the C-terminal transmembrane region of the RYR1 gene. *J. Med. Genet.* 41:e33. doi:10.1136/jmg.2003.014274

Tilgen, N., F. Zorzato, B. Halliger-Keller, F. Muntoni, C. Sewry, L.M. Palmucci, C. Schneider, E. Hauser, F. Lehmann-Horn, C.R. Müller, and S. Treves. 2001. Identification of four novel mutations in the C-terminal membrane spanning domain of the ryanodine receptor 1: association with central core disease and alteration of calcium homeostasis. *Hum. Mol. Genet.* 10:2879–2887. doi:10.1093/hmg/10.25.2879

Tong, J., T.V. McCarthy, and D.H. MacLennan. 1999. Measurement of resting cytosolic Ca2+ concentrations and Ca2+ store size in

HEK-293 cells transfected with malignant hyperthermia or central core disease mutant Ca^{2+} release channels. *J. Biol. Chem.* 274:693–702. doi:10.1074/jbc.274.2.693

Treves, S., H. Jungbluth, F. Muntoni, and F. Zorzato. 2008. Congenital muscle disorders with cores: the ryanodine receptor calcium channel paradigm. *Curr. Opin. Pharmacol.* 8:319–326. doi:10.1016/j.coph.2008.01.005

Ursu, D., R.P. Schuhmeier, M. Freichel, V. Flockerzi, and W. Melzer. 2004. Altered inactivation of Ca^{2+} current and Ca^{2+} release in mouse muscle fibers deficient in the DHP receptor γ1 subunit. *J. Gen. Physiol.* 124:605–618. doi:10.1085/jgp.200409168

Ursu, D., R.P. Schuhmeier, and W. Melzer. 2005. Voltage-controlled Ca^{2+} release and entry flux in isolated adult muscle fibres of the mouse. *J. Physiol.* 562:347–365. doi:10.1113/jphysiol.2004.073882

Wang, X., N. Weisleder, C. Collet, J. Zhou, Y. Chu, Y. Hirata, X. Zhao, Z. Pan, M. Brotto, H. Cheng, and J. Ma. 2005. Uncontrolled calcium sparks act as a dystrophic signal for mammalian skeletal muscle. *Nat. Cell Biol.* 7:525–530. doi:10.1038/ncb1254

Williams, A.J., D.J. West, and R. Sitsapesan. 2001. Light at the end of the Ca^{2+}-release channel tunnel: structures and mechanisms involved in ion translocation in ryanodine receptor channels. *Q. Rev. Biophys.* 34:61–104. doi:10.1017/S0033583501003675

Xu, L., A. Tripathy, D.A. Pasek, and G. Meissner. 1999. Ruthenium red modifies the cardiac and skeletal muscle Ca^{2+} release channels (ryanodine receptors) by multiple mechanisms. *J. Biol. Chem.* 274:32680–32691. doi:10.1074/jbc.274.46.32680

Xu, L., Y. Wang, N. Yamaguchi, D.A. Pasek, and G. Meissner. 2008. Single channel properties of heterotetrameric mutant RyR1 ion channels linked to core myopathies. *J. Biol. Chem.* 283:6321–6329. doi:10.1074/jbc.M707353200

Yang, T., J. Riehl, E. Esteve, K.I. Matthaei, S. Goth, P.D. Allen, I.N. Pessah, and J.R. Lopez. 2006. Pharmacologic and functional characterization of malignant hyperthermia in the R163C RyR1 knock-in mouse. *Anesthesiology.* 105:1164–1175. doi:10.1097/00000542-200612000-00016

Zhao, M., P. Li, X. Li, L. Zhang, R.J. Winkfein, and S.R. Chen. 1999. Molecular identification of the ryanodine receptor pore-forming segment. *J. Biol. Chem.* 274:25971–25974. doi:10.1074/jbc.274.37.25971

Zhou, H., N. Yamaguchi, L. Xu, Y. Wang, C. Sewry, H. Jungbluth, F. Zorzato, E. Bertini, F. Muntoni, G. Meissner, and S. Treves. 2006. Characterization of recessive RYR1 mutations in core myopathies. *Hum. Mol. Genet.* 15:2791–2803. doi:10.1093/hmg/ddl221

Zvaritch, E., F. Depreux, N. Kraeva, R.E. Loy, S.A. Goonasekera, S. Boncompagni, S. Boncompagi, A. Kraev, A.O. Gramolini, R.T. Dirksen, et al. 2007. An Ryr1I4895T mutation abolishes Ca^{2+} release channel function and delays development in homozygous offspring of a mutant mouse line. *Proc. Natl. Acad. Sci. USA.* 104:18537–18542. doi:10.1073/pnas.0709312104

Zvaritch, E., N. Kraeva, E. Bombardier, R.A. McCloy, F. Depreux, D. Holmyard, A. Kraev, C.E. Seidman, J.G. Seidman, A.R. Tupling, and D.H. Maclennan. 2009. Ca^{2+} dysregulation in Ryr1I4895T/wt mice causes congenital myopathy with progressive formation of minicores, cores, and nemaline rods. *Proc. Natl. Acad. Sci. USA.* 106:21813–21818.